Construction and Building Materials 411 (2024) 134411

Contents lists available at ScienceDirect

Construction and Building Materials

journal homepage: www.elsevier.com/locate/conbuildmat

Lateral impact performances of geopolymer concrete columns reinforced with steel-BFRP composite bars

Zhijie Huang [a], Wensu Chen [a,*], Hong Hao [b,a,**], Audrey Ung Siew [a], Tairu Huang [a], Mizan Ahmed [a], Thong M. Pham [c]

[a] Center for Infrastructural Monitoring and Protection, School of Civil and Mechanical Engineering, Curtin University, Australia
[b] Earthquake Engineering Research & Test Center, Guangzhou University, China
[c] UniSA STEM, University of South Australia, Mawson Lakes, SA 5095, Australia

ARTICLE INFO

Keywords:
Geopolymer
Fibre-reinforced concrete
SBCB
Composite bar
Column
Impact loading

ABSTRACT

There is a growing public interest in exploring materials that can enhance the sustainability and durability of conventional steel reinforced concrete (RC) structures, such as geopolymer concrete (GPC) and steel-fibre reinforced polymer composite bars (SFCBs). GPC is produced with industrial waste such as fly ash and slag to replace ordinary Portland cement concrete (OPC), and SFCB is a new reinforcement bar with a layer of fibre reinforced polymer (FRP) enclosing a steel inner core to protect it from corrosion. No studies have ever been reported on the impact-resistant performances of GPC or fibre-reinforced GPC (FRGPC) columns reinforced with SFCBs subjected to vehicle or ship impacts. In this study, GPC/FRGPC columns reinforced with steel-basalt FRP composite bars (SBCBs) were prepared and tested by a pendulum impact testing system. Their impact-resistant performances were compared. It was found that the columns experienced similar damage modes regardless of reinforcement type and fibre content. The addition of hybrid carbon fibres (CFs) and basalt macro fibres (BMFs) could effectively reduce cracking damage and mid height deflections of columns. As compared to steel bar reinforcements, SBCB reinforcements led to similar impact force and maximum mid height deflections, but could reduce the residual mid height deflections of the columns by 7–42% under the impact velocity of 2.64–3.49 m/s, indicating SBCBs have great potential to replace steel bars in constructing more sustainable and durable concrete structures.

1. Introduction

Conventional steel reinforced concrete (RC) structures have the issue of durability due to corrosion of steel reinforcements, leading to costly maintenance and retrofitting for structures, particularly those in coastal areas. Owing to the high corrosion resistance and tensile strength, fibre reinforced polymer (FRP) reinforcements have been gradually being used to replace steel reinforcements in constructions in recent decades [1–3]. However, FRP reinforcements have inherent weaknesses such as brittle behaviour, low modulus of elasticity, and low shear and compressive strengths. The lower modulus of elasticity of FRP bars indicates the lower stiffness of structures, leading to higher deformation of structures under static and impact loads. Additionally, due to their low shear strength, FRP bars in concrete structures may experience splitting damage when subjected to high shear force during impact events, as reported in [4], resulting in more severe damage to concrete structures as compared to those reinforced with steel bars. Moreover, the lower compressive strength of FRP bars contributes to the lower capacity of concrete structures to resist compressive loads. As a result, the use of FRP bars as compression reinforcements is not recommended in the standard ACI 440.1R-15 [5]. Although standard CSA S806–12 [6] allows the use of FRP bars as longitudinal reinforcements in members subjected to axial load, the contribution of compressive strength and stiffness of the FRP bars should be disregarded in design. To address the aforementioned issues with steel and FRP reinforcements, a novel reinforcement known as the steel-FRP composite bar (SFCB) has been proposed in recent years and has received significant attention [7–9].

SFCB is composed of a steel bar as an inner core and a layer of FRP (which can be made of Basalt, Glass, Carbon) as an outer coating, of which the steel core offers the necessary strength and stiffness while the

* Corresponding author.
** Corresponding author at: Earthquake Engineering Research & Test Center, Guangzhou University, China.
E-mail addresses: wensu.chen@curtin.edu.au (W. Chen), hong.hao@curtin.edu.au (H. Hao).

https://doi.org/10.1016/j.conbuildmat.2023.134411
Received 24 August 2023; Received in revised form 10 November 2023; Accepted 30 November 2023
Available online 14 December 2023

FRP coating provides the steel core with additional strength and resistance to corrosion [10]. Using SFCBs benefits concrete structures from the advantages of steel and FRP materials as compared to using either steel or FRP bars alone, and SFCBs showed balanced mechanical properties of steel bars and FRP bars [11]. SFCBs reinforced concrete structures have two potential weak interfaces, i.e., the interface between the steel inner core and FRP coating and the interface between SFCBs and concrete. Previous studies [11,12] demonstrated that the ribbed surface of steel inner core is very effective in developing interfacial bonding strength and a good bonding could be achieved between the ribbed steel inner core and FRP coating [12–14], although strain difference (non-uniform strain distribution) could occur in SFCB cross-section due to the difference in elastic modulus of steel and FRP materials [14]. Testing results [15–17] showed that the bonding strength between SFCBs and concrete under quasi-static load could be comparable or even higher than that between conventional steel bars and concrete, which is affected by various factors such as surface treatment and bar diameter [12,18]. Numerous studies have investigated the mechanical properties of SFCB material [11,12,19] and its bond behaviour with concrete [12, 20–22]. Wu et al. [11] examined the mechanical properties of SFCBs under uniaxial and cyclic tensile loads, proposing analytical models to predict the stress-strain behaviour of SFCBs. Test results by Ma et al. [20] showed that SFCBs had a 47% higher ultimate tensile strength than steel bars and a 169% higher elastic modulus than FRP bars. Moreover, the sand-coated surface of SFCBs exhibited higher bonding strength with concrete and more brittle pullout failure than the spiral-wound surface.

From a structural perspective, the performances of SFCBs reinforced concrete beams [14, 16, 17, 23–27], columns [28–32], and frames [33] under static and seismic loads have been also investigated in recent years. Sun et al. [23], Ge et al. [16], Yang et al. [24], and Han et al. [17] studied the flexural performances of concrete beams reinforced with SFCBs. The results showed that, with the same equivalent reinforcement ratio based on the equal reinforcement stiffness (area × elastic modulus of reinforcements), concrete beams reinforced with SFCBs had similar or better flexural performances than those reinforced solely with either steel or FRP bars in terms of the bending moment capacity, serviceability, and ductility. Analytical methods were proposed for the design analysis of SFCBs reinforced concrete beams [16,17,24]. Besides flexural performances, seismic behaviours of concrete beams reinforced with SFCBs were also investigated. A previous study [25] showed that concrete beams reinforced with SFCBs exhibited a more pronounced pinching effect and a lower residual displacement as compared to those reinforced with steel bars. Xiao et al. [26] conducted a series of tests on different types of SFCBs to evaluate their seismic performances of concrete beams, and found that concrete beams reinforced with steel-basalt FRP composite bars (SBCBs) had higher ultimate capacity and better ductility than those reinforced with steel-glass FRP composite bars (SGCBs) or steel-carbon FRP composite bars (SCCBs). In addition to concrete beams, tests were conducted to investigate the seismic and compressive performances of concrete columns reinforced with SFCBs. The results showed that the columns reinforced with SFCBs had a stable post-yield stiffness after the yielding of the inner steel core, achieved lower residual deformation, and displayed better reparability as compared to those reinforced with steel bars [28,32]. Furthermore, it was found that the ultimate load-bearing capacity of SFCBs reinforced column was greater than that reinforced with FRP bars [30]. These studies suggest that concrete structures reinforced with SFCBs generally exhibit superior performances to those reinforced with steel bars or FRP bars under static or seismic loading, indicating the great potential of SFCBs as an alternative to conventional steel bars in structures under static or seismic loading.

On the other hand, concrete columns might be subjected to impact loading during their service life such as vehicle or ship impacts, which can cause severe damage and potentially catastrophic consequences. It is, therefore, imperative to investigate the performance of concrete columns under impact loading. Geopolymer concrete (GPC), which utilises industrial by-products as binder materials to replace cement and reduce extensive carbon dioxide (CO_2) emissions associated with cement production, is gaining significant attention as a more sustainable alternative to ordinary Portland cement concrete (OPC) [34,35]. A recent study [36] compared the performance of GPC and OPC columns reinforced with BFRP bars or steel bars under impact loading. The results demonstrated that GPC columns had similar or even better impact resistance than OPC columns. Moreover, columns reinforced with BFRP bars outperformed those with steel bars at higher impact velocities (i.e., 3.15–4.43 m/s) due to the higher tensile strength of BFRP bars. However, BFRP bars reinforced columns showed inferior performances at lower impact velocities (i.e., 0–2.71 m/s) due to their lower elastic modulus as compared to steel bars. Huang et al. [37] further examined the effectiveness of reinforcing or strengthening methods on the lateral impact performance of BFRP bars reinforced GPC columns, and found that increasing the longitudinal reinforcement ratio or applying external BFRP sheet strengthening could effectively improve the performance. Given the distinct mechanical properties of longitudinal reinforcements and concrete matrix, GPC/FRGPC columns reinforced with SFCBs might exhibit different impact-resistant performances as compared to the aforementioned columns, which is worthy of studying.

This study aims to assess the effectiveness of SBCBs as an alternative to steel bars in reinforcing GPC columns for impact loading resistance. In this study, six columns (i.e., two GPC columns respectively reinforced with steel bars and BFRP bars as references, one GPC column reinforced with SBCBs, and three FRGPC columns reinforced with SBCBs) were cast and tested by using a pendulum impact testing system. The failure modes and impact responses (impact force and deflection) of the columns were recorded and analysed. Their impact-resistant performances were then compared. The effects of reinforcement type and the addition of hybrid carbon fibres (CFs) and basalt macro fibres (BMFs) on the impact-resistant performances of the GPC columns were investigated.

2. Experimental schemes

2.1. Materials

Table 1 presents the mix design of ambient-cured GPC that was used for the columns. The binder materials comprised fly ash and slag, with slag accounting for 30% of the total binder materials. Alkali activators included a 12 M sodium hydroxide (NaOH) solution and D grade sodium silicate (Na_2SiO_3) solution, with a mass ratio of 1:2.5. Coarse aggregates consisted of crushed stones with a maximum size of 10 mm (50%) and 7 mm (50%), while fine aggregates were natural sands with a maximum size of 1.18 mm. Fig. 1 illustrates the longitudinal reinforcements (steel bars, BFRP bars, and SBCBs) used in this study, all of which have a diameter of 10 mm. The representative stress-strain curves for steel bars, BFRP bars, and SBCBs are presented in Fig. 2, which are provided by the supplier [38]. The yield strength and elastic modulus of steel bars are around 500 MPa and 210 GPa, respectively. The tensile strength, elastic modulus, and elongation of BFRP bars are about 1200 MPa, 50 GPa, and 2.4%, respectively. SBCBs show a bi-linear stress-strain behaviour until ultimate strength. The initial elastic modulus and post-yielding modulus of SBCB are about 100 GPa and 30 GPa, respectively. Its inner steel core yields at around 250 MPa until reaching the ultimate tensile strength of 900 MPa. In general, the tensile strength and elastic modulus of SBCBs are in between those of steel bars and BFRP bars. Once the outer BFRP layer ruptures, the axial force is sustained by the yielded steel core until

Table 1
Mix proportion of ambient-cured GPC (kg/m^3) [39].

Coarse aggregates	Sand	Binder		Solution		Alkaline solution/ binder ratio
		Fly ash	Slag	Na_2SiO_3	NaOH	
1220	650	280	120	129	51	0.45

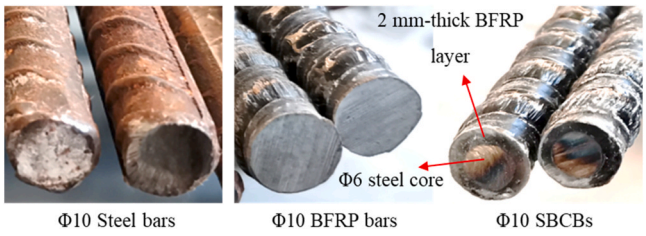

Fig. 1. Longitudinal reinforcements of the columns.

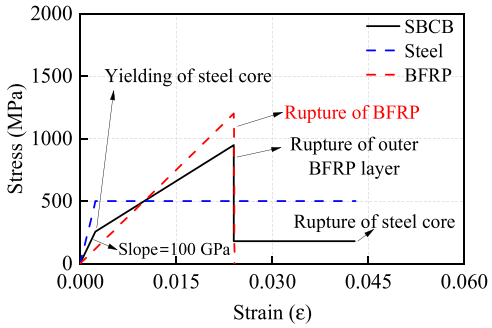

Fig. 2. Stress-strain curves of longitudinal reinforcements.

it also ruptures.

As mentioned in reference [40], micro fibres can bridge microcracks and improve the first cracking strength, while macro fibres can arrest the propagation of macro cracks and enhance the post-cracking performance of concrete. The combination of micro and macro fibres benefits concrete strength by influencing crack growth at different stages [41]. Therefore, CFs (carbon fibres) were chosen as micro fibres and BMFs (basalt macro fibres) were selected as macro fibres for reinforcing geopolymer concrete due to their sound corrosion resistance and tensile strength. Fig. 3 shows the fibres used in this study. BMFs have a density of 2000 kg/m^3, a length of 50 mm, and a diameter of 0.65 mm, with an aspect ratio (length to diameter) of 77. Their tensile strength and modulus of elasticity are about 1200 MPa and 50 GPa, respectively, as provided by the supplier [38]. According to reference [42], using BMF content exceeding 40 kg/m^3 (about 2% by volume fraction) can lead to the difficulty of concrete compaction. Hence, a volume fraction of 0 (column C3, as listed in Tables 2), 1% (column C4), and 2% (maximum fibre content, column C5) for BMFs was adopted in this study. The CFs used in this study have a length of 6 mm and a diameter of 7 μm. The density, tensile strength, tensile modulus of elasticity, and elongation of CFs are approximately 1800 kg/m^3, 3500 MPa, 230 GPa, and 1.5%, respectively, as provided by supplier [38]. A previous study [43] demonstrated that a volume fraction of 0.25% of CFs yielded good performance for concrete. Therefore, a CF content of 0.25% (columns C4 and C5) was used in this study. Besides the benchmark of hybrid 0.25% CF and 2% BMF (column C5), the combination of 0.31% CF and 1.5% BMF (column C6), with 25% increment of CF and 25% decrement of BMF content, was also considered, as listed in Table 2.

Fig. 3. Basalt macro fibres (left) and carbon fibres (right).

2.2. Specimens

In this study, a total of six columns were cast and tested by using a pendulum impact testing system. Table 2 gives the details of the columns. Columns C1 and C2 were longitudinally reinforced with steel and BFRP bars, respectively, as references to column C3 that was longitudinally reinforced with SFBCs without the addition of fibres. Columns C4-C6 were made of FRGPC with different fibre contents as described above. It should be noted that the slight difference in the compressive strengths of the GPC of the columns was due to the different batches of GPC casting. Fig. 4 shows the design of the columns. The column had a square cross-sectional dimension of 120 mm × 120 mm and a height of 800 mm. A footing and a top slab were connected to the column. Four 10 mm-diameter steel bars/BFRP bars/SBCBs were used as longitudinal reinforcements and sixteen 10 mm-diameter BFRP stirrups were used as transverse reinforcements at a space of 50 mm. The longitudinal reinforcement ratio of the columns was 2.2% and the stirrup ratio was 2.6%. C3 had an estimated axial load-carrying capacity of 710 kN (without considering the contribution of BFRP layer of SBCBs) according to ACI 318–14 [44]. Since no analysis and design standard is available for concrete structures reinforced with SBCBs, the flexural and shear capacities of C3 were estimated as per ACI 440.1R-15 (the design guide for FRP reinforced concrete structures) [5]. Its flexural capacity at column base section (critical section) was estimated as 7 kNm (corresponding to an equivalent static force of 17.5 kN acting at the mid height) and its shear capacity was estimated as 66 kN. It should be noted that bend SBCBs are unavailable due to the limitation of current manufacturing techniques. Therefore, additional four BFRP dowels with a 90-degree round angle were used to reinforce the connections between the column and footing/top slab for the adequate anchorage of the longitudinal reinforcements inside concrete.

2.3. Test setup

Fig. 5 shows the pendulum impact testing system. The whole column was secured to a concrete base that was firmly anchored to the ground. An added weight, composed of two concrete blocks weighing 720 kg, was bolted onto the top slab, which is mainly for the consideration of the inertial effect of superstructures of columns. To ensure no slip or sliding between the added weight and top slab, four thru-holes were prepared for the top slab to anchor the additional weight using bolts as shown in Fig. 5. The axial load applied to the column by the gravity of the added weight was approximately 1% of the axial load-bearing capacity, which was relatively low due to the limitations imposed by the laboratory conditions. During the tests, a 373 kg impactor was lifted and released, striking the columns at the mid height location. The pendulum arm had a length of 2.7 m. The columns were subjected to four repetitive impacts with increasing impact velocities. Different impact angles of 5°, 15°, 30°, and 40° with the corresponding impact velocities of 0.45 m/s, 1.33 m/s, 2.64 m/s, and 3.49 m/s (listed in Table 2) were selected to yield varying levels of damage to the columns. A load cell was incorporated in the front of the impactor to measure the impact force, and linear variable differential transformers (LVDTs) were used to record the displacements and free vibration period of the columns. Additionally, a high-speed camera was used to capture the failure progress of the columns.

3. Test results and analysis

3.1. Crack patterns of the columns

Fig. 6 depicts the damage modes and crack patterns of the columns

Table 2
Specimens and testing schemes of the columns.

Column No.	Compressive strength f_c' (MPa)	Longitudinal reinforcement type	Fibre content by volume fraction (%)	Number of impacts	Designed four impact velocities (m/s)
C1	63	Steel	0	4	0.45 (5°),
C2	57	BFRP	0		1.33 (15°),
C3	54	SBCB	0		2.64 (30°),
C4	50	SBCB	CF: 0.25 + BMF: 1.0		3.49 (40°)
C5	54	SBCB	CF: 0.25 + BMF: 2.0		
C6	52	SBCB	CF: 0.31 + BMF: 1.5		

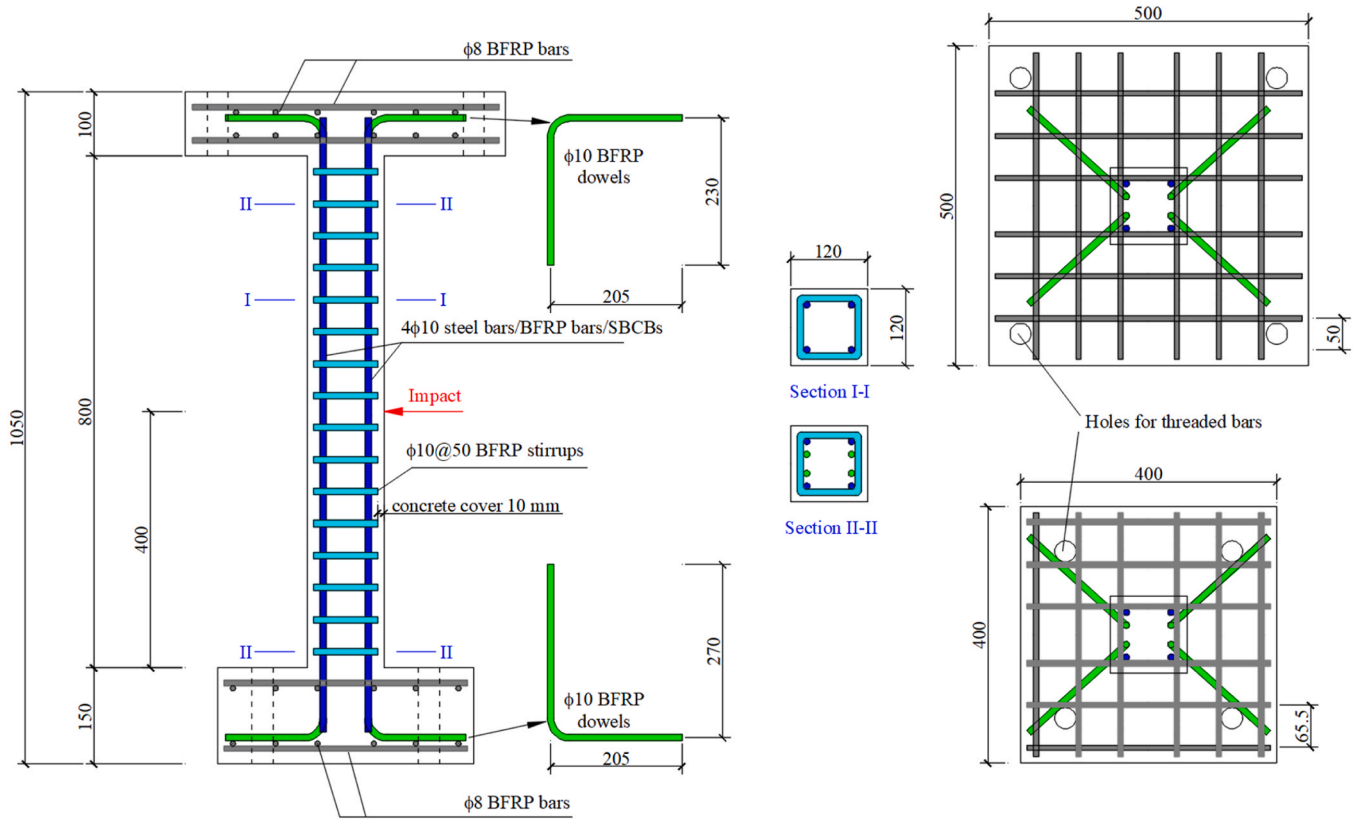

Fig. 4. Column design diagram.

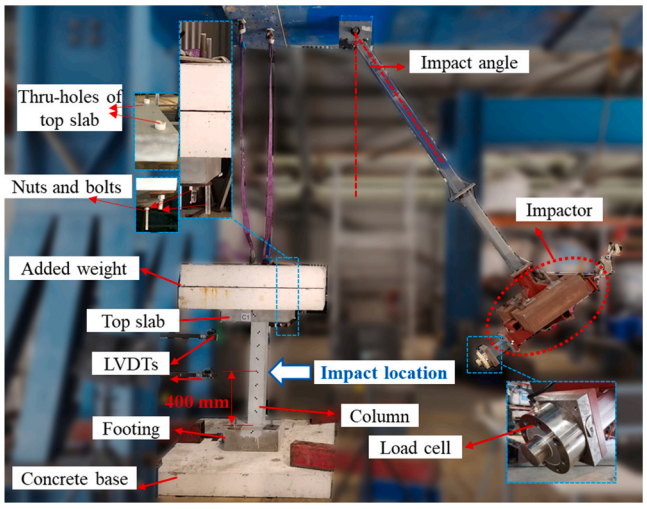

Fig. 5. Photograph of the pendulum impact testing system.

after each impact. It should be noted that there were pre-existing hairline cracks on the columns, which are often difficult to be avoided during the processes of formwork demoulding and specimen relocation. After the impact of velocity 0.45 m/s, no visible crack was observed on all the tested columns. After the impact of velocity 1.33 m/s, only hairline flexural cracks appeared near the mid height areas of the columns due to local bending. The damage to the columns was negligible, and the cracking patterns of the columns were flexure dominant. After the impact of velocity 2.64 m/s, the existing flexural cracks became wider and longer, and additional flexure-shear cracks or shear cracks appeared in the mid height areas due to the rising impact velocity. Meanwhile, a few flexural cracks or flexure-shear cracks were also observed at the bottom of the columns due to global bending. It should be noted that some flexure and shear cracks were also observed at the top of columns as shown in Fig. 7 (captured by the high-speed camera during crack opening stage), due to the high bending moment and shear force at the top of columns as reported in [37]. Most of these cracks are not visible in Fig. 6 because they closed after impacts. After the 4th impact (3.49 m/s), the crack patterns at the mid height of columns had no significant change except that a few secondary cracks occurred, and the existing cracks grew wider. All the columns experienced varying degrees of concrete crushing and spalling damage at the impact location

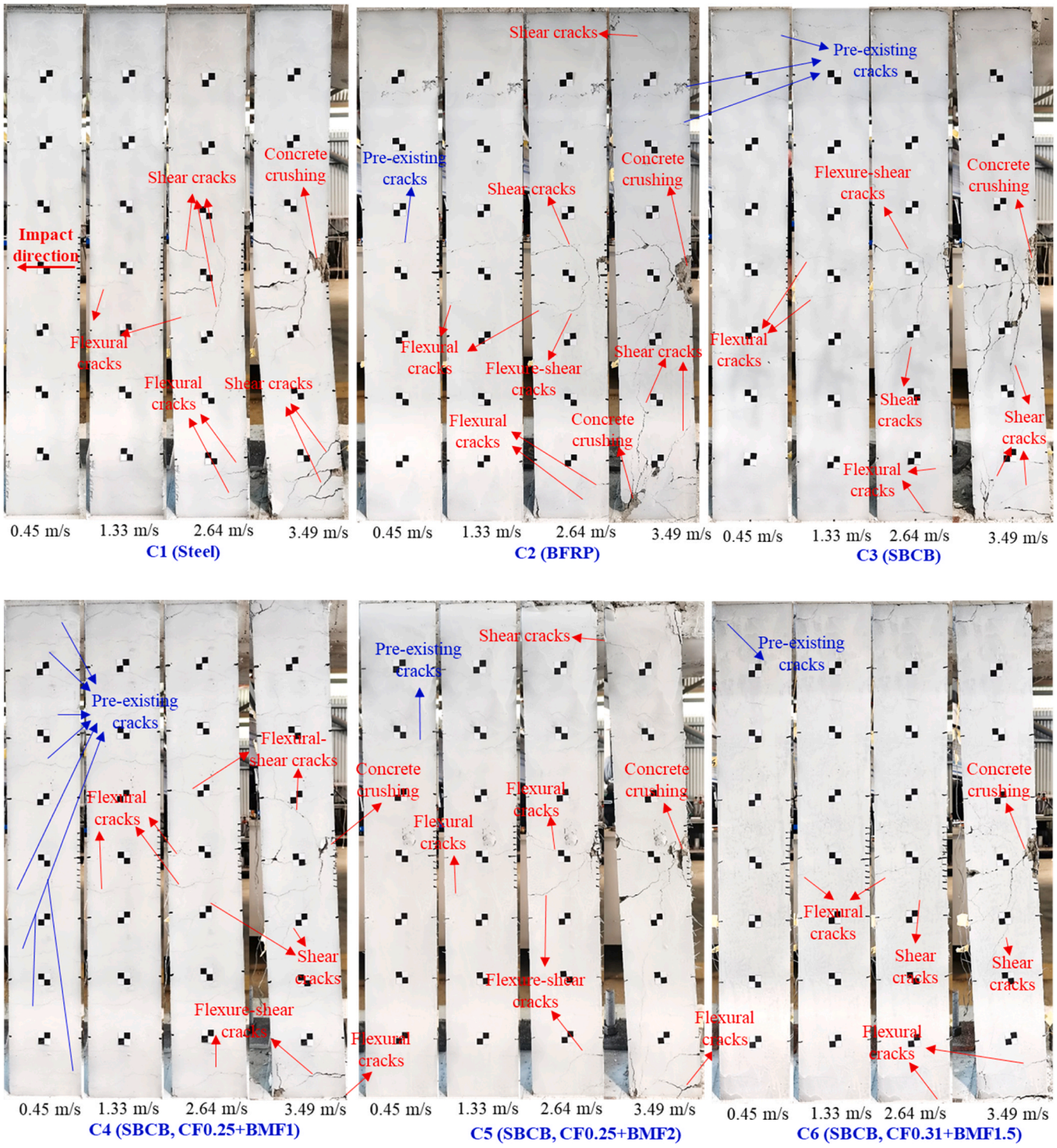

Fig. 6. Damage modes of the columns.

as shown in Fig. 8. The addition of fibres effectively reduced the crushing and spalling damage of the columns at impact location. At the column bottom, several shear cracks were observed on columns C1-C3 due to the increased shear force, and minor concrete crushing damage was also observed on the compressive side of column C2 at the bottom. In contrast, only some new flexural cracks were developed at the bottom of columns C4-C6. Overall, all the columns experienced similar cracking damage, i.e., flexure-dominant cracking damage at relatively low impact velocities (0.45–1.33 m/s) and flexure-shear combined cracking damage at relatively high impact velocities (2.64–3.49 m/s) regardless of reinforcement type. As compared to the GPC column without fibres (C1-C3), FRGPC columns C4-C6 exhibited less cracking and concrete crushing and spalling damage.

3.2. *Damage progression*

Fig. 9 describes the damage progression of the columns captured by the high-speed camera. Due to the negligible damage of the column at 0.45 m/s and 1.33 m/s, the damage progression of the columns under these two impacts is not shown herein. Under the 3rd impact (2.64 m/s),

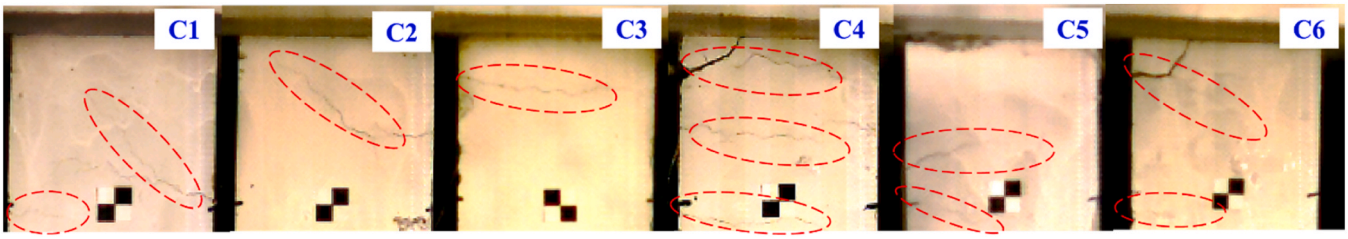

Fig. 7. Cracks at the top of columns during impact.

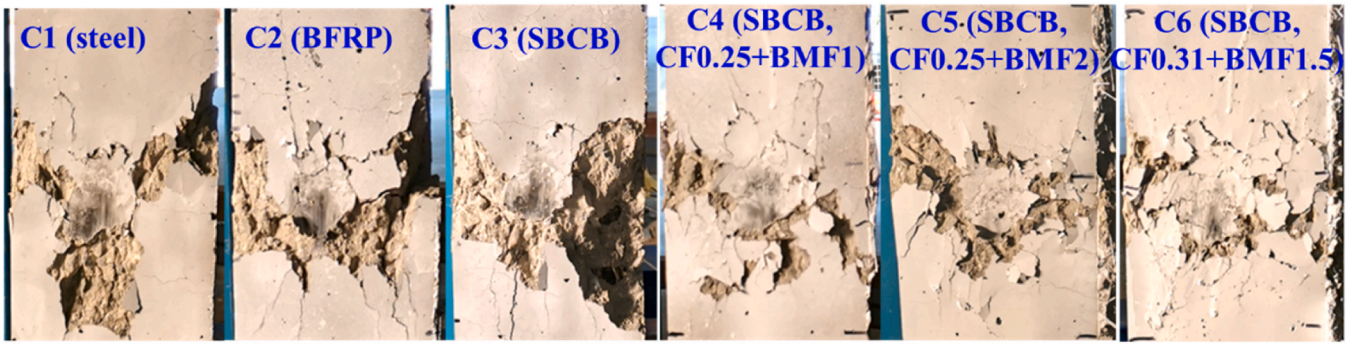

Fig. 8. Damage at impact location.

some new flexural cracks initiated at 1 ms (millisecond) on all the columns. These cracks then became more visible over time. The main crack patterns were formed at 4 ms and no significant changes were observed at 10 ms and 70 ms except the extension of the cracks. Under the 4th impact (3.49 m/s), all the columns experienced minor concrete crushing damage at the impact location at 4 ms and concrete debris spalled from the columns without fibres. In the mid height areas, the existing cracks of columns opened wider, while the critical crack patterns almost remained the same. In the bottom areas, more shear cracks were observed on columns C1-C3 during 4–10 ms, leading to the flexure-shear combined cracking damage modes at the bottom of the columns. In contrast, a flexural crack appeared at the bottom of columns C4 and C6, and the existing flexural cracks near the bottom of column C5 further opened and extended, resulting in flexural cracking damage modes at the bottom of these three columns. Generally, the reinforcement type showed an insignificant effect on the damage progression of columns. The addition of fibres led to more evident cracking damage (crack opening) at the bottom of columns due to global bending as compared to those without fibres.

3.3. Impact force

The impact forces and responses of the columns are summarized in Table 3 and the time histories of impact forces are shown in Fig. 10(a)-(d). All the columns experienced very similar profiles of impact force regardless of reinforcement type and fibre content. The impact forces show two main peaks, which could also be found in the references [45,46]. The impact force increases to the first main peak, followed by a decrease and then an increase to the second main peak. The first main peak drops to a low level at the specific time instant of 1.1–1.2 ms. This phenomenon can be attributed to the asynchronous acceleration and deceleration processes of the column and impactor, which can be explained as follows. When the displacement (d_i) of impactor exceeds that of the column (d_c), resulting in an indentation on the column surface as shown in Fig. 11, an impact force is generated. If the velocity (v_i) of the impactor is higher than that of the column (v_c), the impact force increases, and vice versa.

Due to the complexity of interaction between the impactor and column, numerical simulation was employed to assist in revealing these processes. A numerical model of a GPC column reinforced with BFRP bars, subjected to impact loading as shown in Fig. 12(a), was generated in LS-DYNA for this purpose. This numerical model, whose accuracy has been validated against testing results, was adopted from the previous studies [36,37]. Detailed information about the numerical model can be found in the references [36,37] and is not reiterated herein for brevity. As shown in Fig. 12(b), the impact force from numerical simulation also shows two main peaks, with the first pulse lasting for 1.1 ms, which is consistent with the testing results of this study. Specifically, the impact force increases during 0–0.53 ms when $v_i - v_c > 0$, and decreases during 0.53–1.1 ms when $v_i - v_c < 0$, further confirming the asynchronous acceleration and deceleration processes between the column and impactor, as mentioned earlier. It is worth noting that the double-peak phenomenon of impact force is influenced by the factors such as the shape of the impact surface, contact stiffness, and the stiffness of objects subjected to impact loading [47]. For instance, the flatter the contact surface, the more evident the double-peak phenomenon [47].

At relatively low impact velocities (e.g., 0.45–1.33 m/s), the first main peak was much lower than the second main peak, which might be due to the low inertial force associated with the low impact velocity. At relatively high impact velocities (e.g., 2.64–3.49 m/s), the first main peak increased to a similar magnitude to the second main peak, which could be due to the increased inertial force. In addition, the duration of impact force of column C1 was slightly shorter than those of other columns due to the higher stiffness of steel reinforcements. Fig. 10(f) gives the peak impact forces of the columns for each impact. The peak impact forces of column C1 were the highest, followed by column C2 and other columns due to the higher compressive strength of concrete as tabulated in Table 2. Columns C3-C6 experienced very similar peak impact forces under all impacts due to the similar compressive strengths of concrete (50–54 MPa). Overall, the impact forces of the columns exhibited a similar trend and their peak values fell within a consistent range, with a relative difference of less than 24% observed across all reinforcement types. The addition of hybrid CFs up to 0.31% and BMFs up to 2% by volume fraction has a negligible effect on the impact forces. This observation is understandable since the addition of these fibres had negligible influence on the compressive strength of concrete and thus

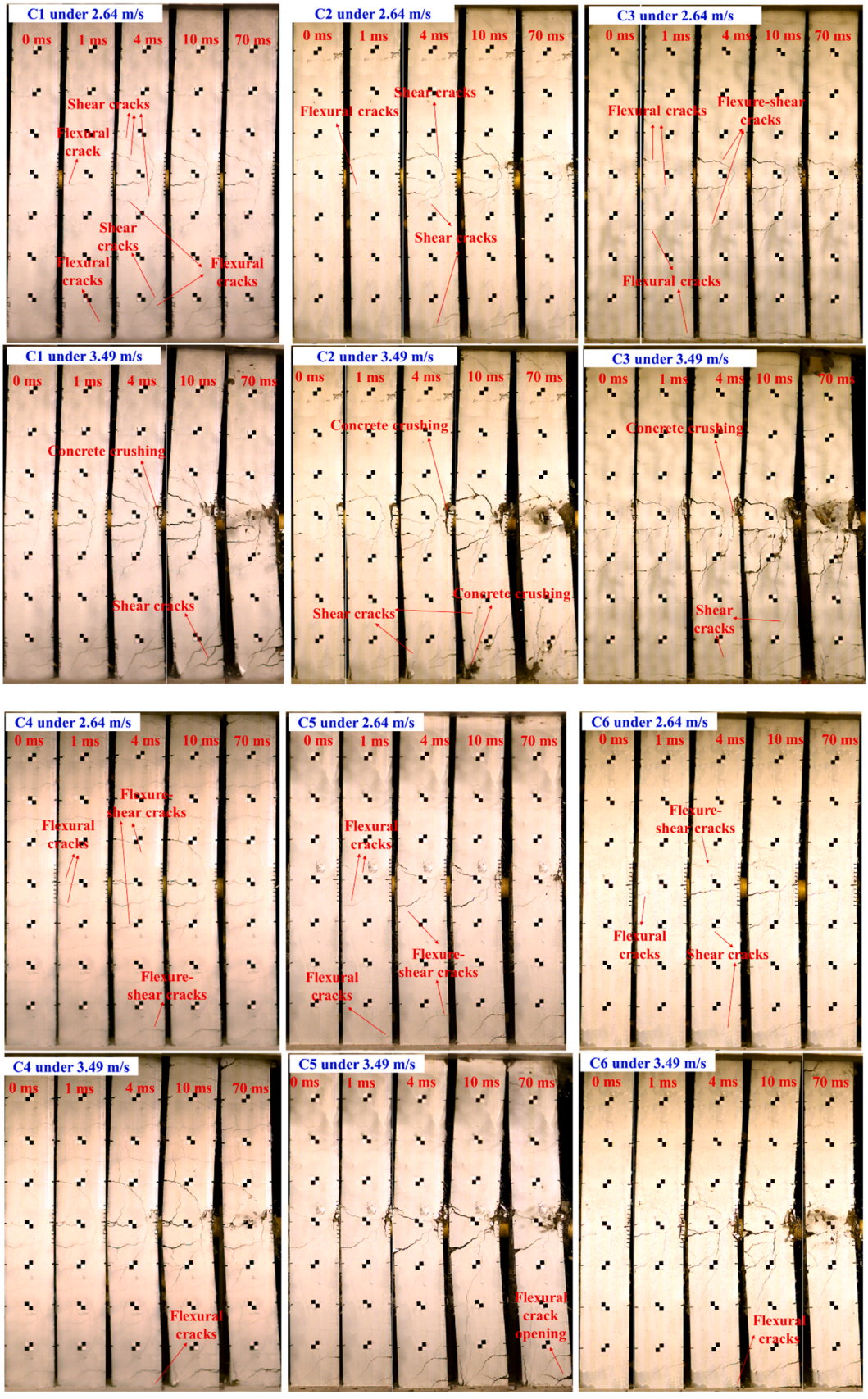

Fig. 9. Damage progression of the columns.

Table 3
Impact test results of the columns.

Specimen	Impact No.	Designed impact velocity (m/s)	Peak impact force (kN)	Maximum mid height deflection (mm)	Residual mid height deflection (mm)	Free vibration period (s)
C1	1 (5°)	0.45	28.1	0.9	0.0	0.33
	2 (15°)	1.33	72.3	4.9	0.2	0.37
	3 (30°)	2.64	113.6	15.8	5.3	0.40
	4 (40°)	3.49	124.6	31.2	19.6	0.45
C2	1 (5°)	0.45	25.3	1.2	0.2	0.40
	2 (15°)	1.33	61.8	7.6	1.1	0.46
	3 (30°)	2.64	100.2	16.9	3.0	0.54
	4 (40°)	3.49	113.8	29.9	13.1	0.64
C3	1 (5°)	0.45	21.3	1.0	0.1	0.39
	2 (15°)	1.33	59.1	5.0	1.0	0.46
	3 (30°)	2.64	100.1	16.1	3.1	0.53
	4 (40°)	3.49	111.8	30.8	18.2	0.55
C4	1 (5°)	0.45	24.4	1.5	0.0	0.40
	2 (15°)	1.33	57.5	6.7	0.1	0.47
	3 (30°)	2.64	90.7	17.4	3.2	0.60
	4 (40°)	3.49	109.5	30.5	15.1	0.62
C5	1 (5°)	0.45	24.3	1.0	0.0	0.35
	2 (15°)	1.33	56.7	4.8	0.6	0.44
	3 (30°)	2.64	93.9	13.0	3.5	0.53
	4 (40°)	3.49	111.1	28.3	17.3	*
C6	1 (5°)	0.45	23.0	1.0	0.0	0.37
	2 (15°)	1.33	58.4	4.8	0.1	0.46
	3 (30°)	2.64	98.5	14.0	2.8	0.53
	4 (40°)	3.49	113.9	28.7	20.5	0.58

Note: "* " no recorded data.

the contact stiffness of these columns.

3.4. Mid height deflection

Fig. 13 shows the time histories of the lateral deflection at mid height of the columns. All columns experienced three stages during the whole impact process as indicated in Fig. 13(a) (stages A, B, and C). During stage A, the columns accelerated by an external force (impact force) and the mid height deflection of the columns increased. After the impact force decreased to zero (separation between columns and impactor, before 40 ms according to Fig. 10), the mid height deflection of columns still increased due to the inertial effect until the velocity decreased to zero and the deflection reached peak value. After that, the mid height deflection of columns decreased until about 60 ms for the case with impact velocity 0.45 m/s (Fig. 13(b)), 80 ms for the case with impact velocity 1.33 m/s (Fig. 13(c)), 100 ms for the case of 2.64 m/s impact (Fig. 13(d)), and 120 ms for the case of 3.49 m/s impact (Fig. 13(f)), and it then increased again (during stage B) due to the inertial force of added weight. Finally, the columns entered into the free vibration stage (stage C) after about 380–600 ms. All the columns exhibited similar deflection trend with slightly different free vibration frequencies.

The maximum and residual mid height deflections of the columns are summarized in Fig. 14. Among columns C1-C3, C1 exhibited the lowest maximum mid height deflections for the cases with impact velocity 0.45–2.64 m/s due to the higher flexural stiffness of the column associated with the elastic modulus of the reinforcements, followed by columns C3 and C2. Similarly, C1 experienced the lowest residual mid height deflections when the impact velocities were 0.45–1.33 m/s as shown in Fig. 14(b), followed by C3 and C2. This finding is in agreement with the conclusions in reference [36]. With higher impact velocity, column C2 experienced the lowest maximum mid height deflection (29.9 mm) for the case with impact velocity 3.49 m/s as BFRP bars still remained in elastic, followed by column C3 (30.8 mm) and column C1 (31.2 mm) due to the yielding of steel bars. Owing to the same reason, C2 experienced the lowest residual mid height deflections when the impact velocities were 2.64–3.49 m/s as shown in Fig. 14(b). For the columns without fibre reinforcement, using SBCBs could achieve very similar maximum mid height deflections of the columns when impacted at velocities of 0.45–3.49 m/s and the residual mid height deflections of the columns were 7–42% smaller for the cases with impact velocities 2.64–3.49 m/s, as compared to steel bars.

Among columns C3-C6, column C5 generally experienced the lowest mid height deflection due to the bridging effect of hybrid fibres, followed by C6, C4, and C3. However, column C4 had slightly higher maximum mid height deflections than column C3 for the cases with impact velocities 0.45–2.64 m/s, which might be due to the lower stiffness of column C4 resulting from the more severe pre-existing cracks (see Fig. 6) induced in the processes of formwork demoulding and specimen relocation as mentioned above. Generally, FRGPC columns (C4-C6) yielded lower residual mid height deflections than the column without fibres (C3) except C4 and C5 in the case with impact velocity 2.64 m/s and C6 with impact velocity 3.49 m/s, which might be due to the resistance of fibres at cracks preventing the closure of cracks as reported in reference [37]. By comparing the testing results of C5 and C6, it can be found that increasing the volume fraction of CFs while decreasing the volume fraction of BMFs generally led to slightly higher maximum and residual mid height deflections, which demonstrates that BMFs are more effective in arresting crack opening than CFs. To conclude, with the addition of BMFs up to 2% by volume fraction, the maximum and residual mid height deflections of the columns could be reduced by up to 19% and 90% when impacted with velocities of 0.45–3.49 m/s, respectively.

Fig. 15 shows the free vibration period of the columns, which is illustrated in Fig. 13(a). It should be noted that the free vibration period of column C5 at 3.49 m/s was not captured due to the malfunction of LVDT, and thus is not presented herein. The free vibration period is primarily dependent on the residual stiffness of the columns. The shorter free vibration period implies the higher residual stiffness of the columns. The residual stiffness of the columns is contributed by concrete and reinforcements together. As seen, the free vibration periods of the columns increase with the number of impacts, which is due to the cumulated damage of the column after every impact, leading to the decrease of stiffness of the columns. As expected, column C1 had the shortest free vibration periods due to the highest stiffness of the longitudinal reinforcements, followed by columns C3 and C2 among these three columns. Among columns C3, C5 and C6, column C5 generally showed the

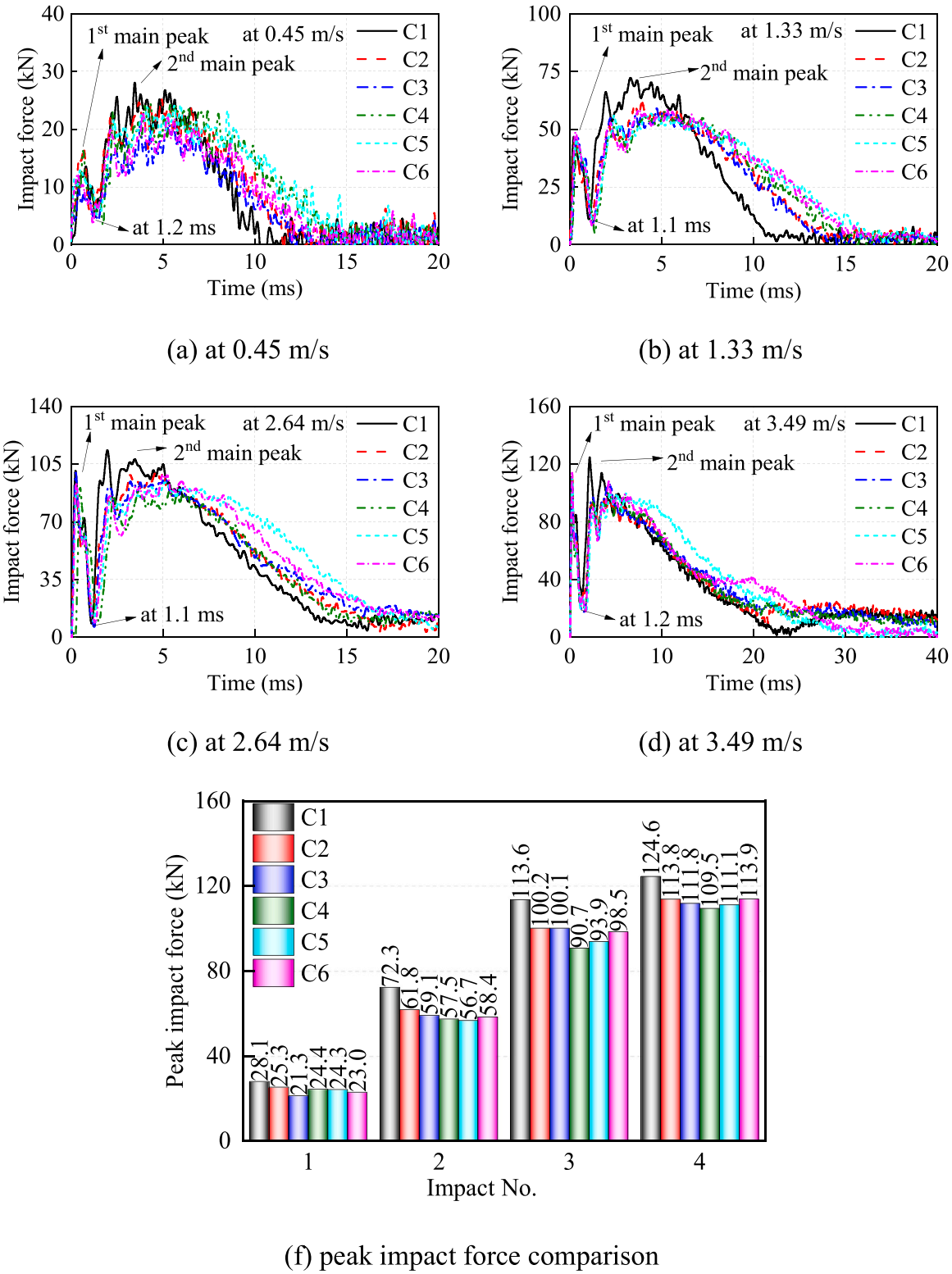

Fig. 10. Impact force time histories from experimental testing.

shortest free vibration period, followed by C6 and C3 except C6 under the 4th impact (3.49 m/s). It can be concluded that the addition of hybrid CFs and BMFs could enhance the stiffness of columns, which further led to lower maximum mid height deflections of columns as shown in Fig. 14(a). Column C4 exhibited slightly longer free vibration periods than columns C3, C5 and C6 due to the lower stiffness caused by pre-existing cracks as mentioned above. The trend of free vibration periods in Fig. 15 is consistent with that of maximum mid height deflections in Fig. 14(a), which confirms the accuracy of the results.

4. Conclusion

In this study, six columns (i.e., two GPC columns respectively reinforced with steel bars or BFRP bars as references, one GPC column

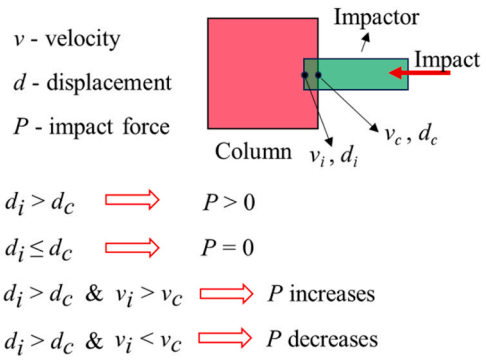

Fig. 11. Illustration of generation of impact force (subscript 'i' represents impactor, 'c' represents column).

reinforced with SBCBs, and three FRGPC columns reinforced with SBCBs) were prepared and tested by using a pendulum impact testing system. Their impact-resistant performances were examined in terms of damage patterns, failure progression, impact forces, mid height deflections, and free vibration period. The effects of longitudinal reinforcement type and hybrid fibre content on the impact-resistant performances of the columns were also studied. Based on the testing results, the following conclusions are drawn.

1. The use of different longitudinal reinforcement types and fibre contents in GPC columns did not affect the interaction of column with the impactor, and as a result, the impact forces experienced by the column and the column damage modes, i.e., flexure-dominant cracking damage at relatively low impact velocities (0.45–1.33 m/s) and flexure-shear combined cracking damage at relatively high impact velocities (2.64–3.49 m/s) for all the columns were similar.
2. Reinforcing columns with SBCBs resulted in very similar maximum mid height deflections of columns as those reinforced with conventional steel bars when the columns were impacted with velocities of 0.45–3.49 m/s, but smaller residual mid height deflections of columns when impacted at velocities of 2.64–3.49 m/s; the reduction in the residual deflection was in the range of 7–42%.
3. The use of CFs and BMFs in reinforcing GPC reduced the cracking damage of columns and increased the stiffness of columns, which led to a more evident global bending damage at the bottom of columns, and therefore should be carefully considered when designing FRGPC columns that are subjected to impact loading.
4. BMFs were more effective in arresting crack openings than CFs. With the addition of BMFs up to 2% by volume fraction, the maximum and residual mid height deflections of columns were up to 19% and 90% smaller than the columns without fibre reinforcement when impacted with velocities of 0.45–3.49 m/s, respectively.
5. Overall, the columns reinforced with SBCBs showed similar cracking damages and comparable structural responses or even lower residual mid height deflections than those reinforced with steel bars. Therefore, SBCBs and GPC are promising alternatives to steel bars and OPC, respectively, for more durable concrete structures for impact loading resistance.

In this study, the scaled-down columns were tested to investigate the effect of reinforcement type and fibre content on the impact responses of the columns, which is the main objective of this study. With the numerical model calibrated against the testing results in the present study, large-scale column/pier numerical models could be built and their performance under various loading conditions could be investigated.

CRediT authorship contribution statement

Huang Zhijie: Writing – original draft, Methodology, Investigation, Formal analysis, Data curation, Conceptualization. **Chen Wensu:** Writing – review & editing, Validation, Supervision, Methodology, Conceptualization, Project administration. **Hao Hong:** Writing – review & editing, Supervision, Resources, Funding acquisition, Conceptualization. **Siew Audrey Ung:** Investigation, Data curation. **Huang Tairu:** Investigation, Data curation. **Ahmed Mizan:** Writing – review & editing.

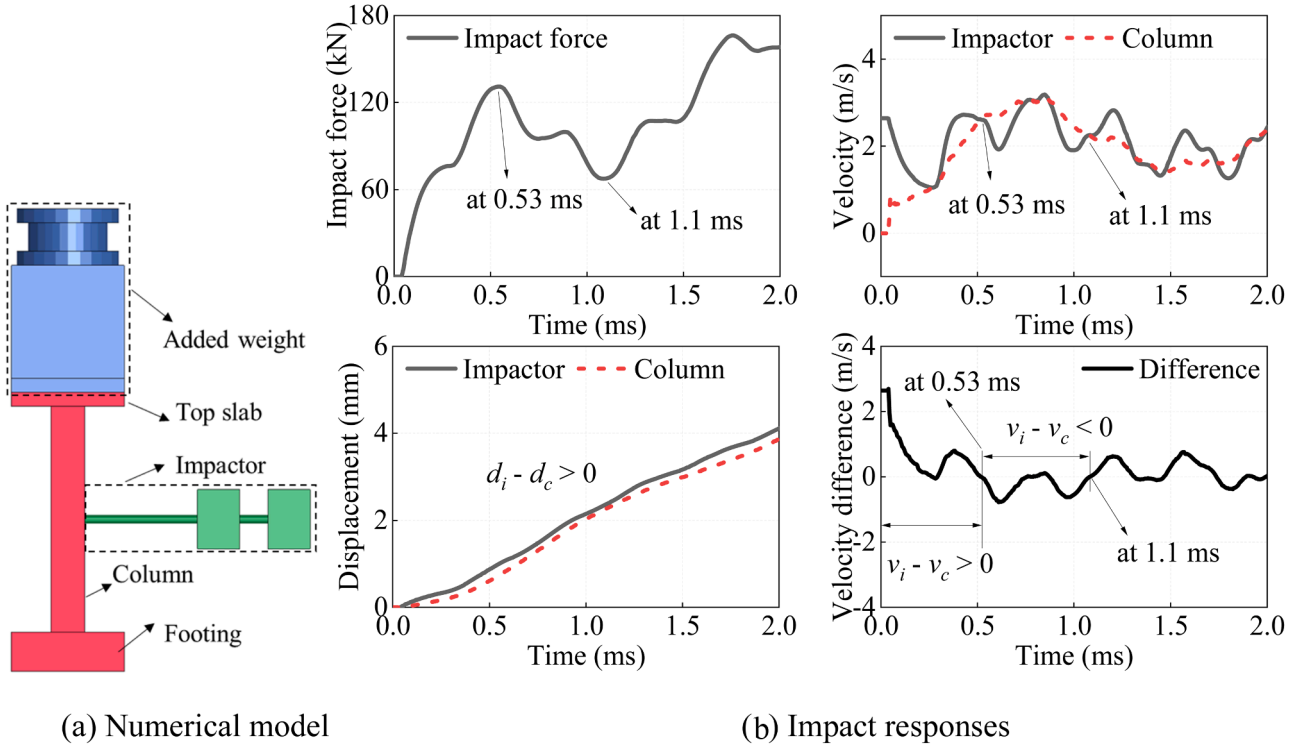

Fig. 12. Interaction between impactor and column (numerical results).

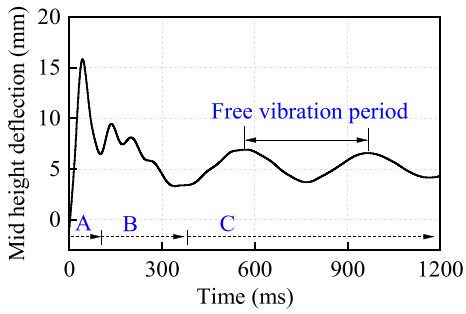

(a) illustration of three stages of deflections

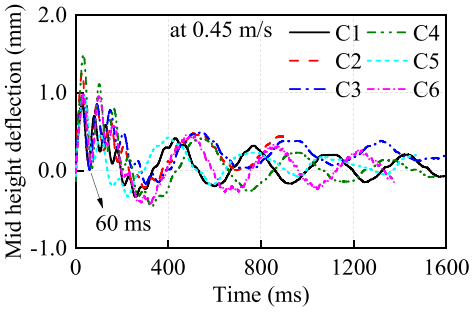

(b) 0.45 m/s impact

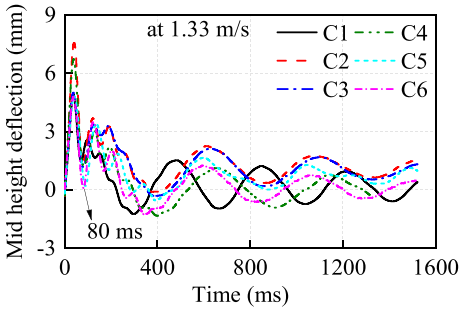

(c) 1.33 m/s impact

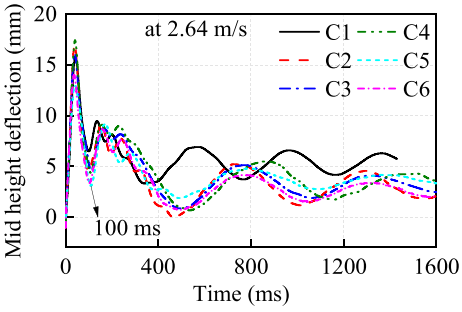

(d) 2.64 m/s impact

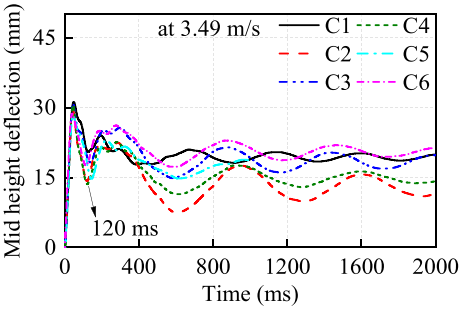

(e) 3.49 m/s impact

Fig. 13. Time histories of mid height deflection responses.

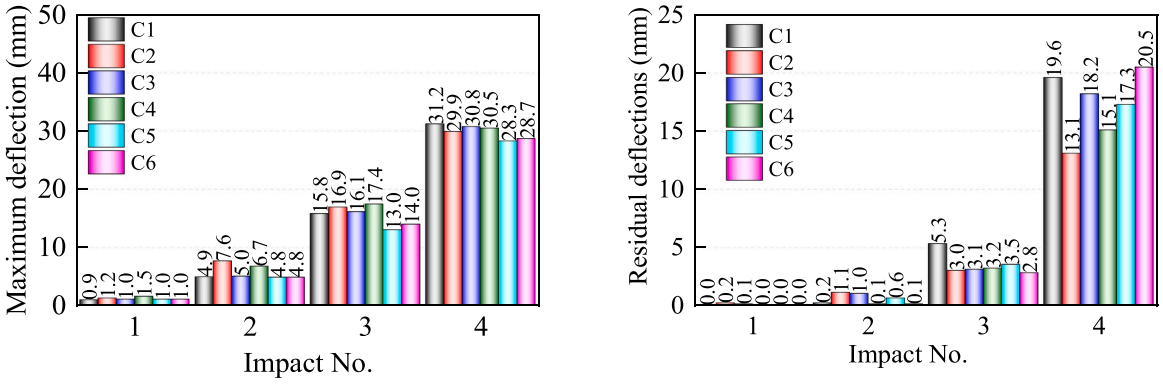

(a) maximum deflections (b) residual deflections

Fig. 14. Maximum and residual mid height deflections.

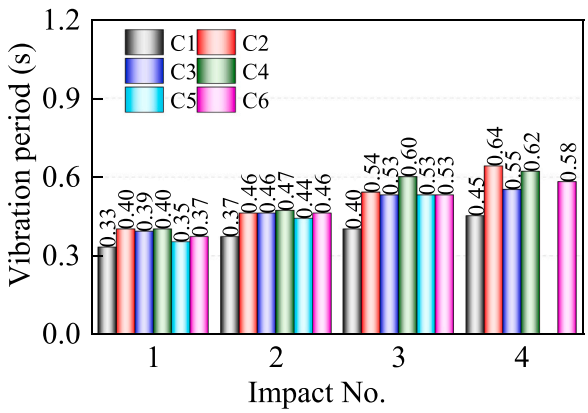

Fig. 15. Free vibration periods of columns.

Pham Thong M.: Writing – review & editing.

Acknowledgements

The financial support from the Australian Research Council (ARC) via Australian Laureate Fellowship (FL180100196) is greatly appreciated.

Declaration of Competing Interest

The authors declare that they have no known competing financial interests or personal relationships that could have appeared to influence the work reported in this paper.

Data Availability

Data will be made available on request.

References

[1] Amran Y.M., Alyousef R., Rashid R.S., Alabduljabbar H., Hung C.-C. Properties and applications of FRP in strengthening RC structures: A review. Structures. 2018.
[2] Z. Huang, W. Chen, T.T. Tran, T.M. Pham, H. Hao, Z. Chen, et al., Experimental and numerical study on concrete beams reinforced with Basalt FRP bars under static and impact loads, Compos Struct. 263 (2021), 113648.
[3] H. Hao, K. Bi, W. Chen, T.M. Pham, J. Li, Towards next generation design of sustainable, durable, multi-hazard resistant, resilient, and smart civil engineering structures, Eng. Struct. 277 (2023), 115477.
[4] Z. Huang, W. Chen, H. Hao, Z. Chen, T.M. Pham, T.T. Tran, et al., Shear behaviour of ambient cured geopolymer concrete beams reinforced with BFRP bars under static and impact loads, Eng. Struct. 231 (2021), 111730.
[5] ACI 440.1R-15. Guide for the design and construction of concrete reinforced with Fiber Reinforced Polymers (FRP) bars. Farmington Hills, MI, USA: American Concrete Institute; 2015.
[6] CSA S806–12. Design and construction of building structures with fibre-reinforced polymers. Ontario, Canada: Canadian Standards Association; 2012.
[7] W.-J. Ge, J.-w Zhu, A. Ashour, Z.-P. Yang, X.-n Cai, S. Yao, et al., Effect of Chloride Corrosion on Eccentric-Compression Response of Concrete Columns Reinforced with Steel-FRP Composite Bars, J. Compos Constr. 26 (2022).
[8] L. Wang, L. Fan, F. Fu, Z. Song, Cracks width prediction of steel-FRP bars reinforced high-strength composite concrete beams, Structures 43 (2022) 424–433.
[9] Y. Zhou, H. Gao, Z. Hu, Y. Qiu, M. Guo, X. Huang, et al., Ductile, durable, and reliable alternative to FRP bars for reinforcing seawater sea-sand recycled concrete beams: steel/FRP composite bars, Constr. Build. Mater. 269 (2021).
[10] Y. Zhou, Y. Zheng, J. Pan, L. Sui, F. Xing, H. Sun, et al., Experimental investigations on corrosion resistance of innovative steel-FRP composite bars using X-ray microcomputed tomography, Compos Part B-Eng. 161 (2019) 272–284.
[11] G. Wu, Z.-S. Wu, Y.-B. Luo, Z.-Y. Sun, X.-Q. Hu, Mechanical properties of steel-FRP composite bar under uniaxial and cyclic tensile loads, J. Mater. Civ. Eng. 22 (2010) 1056–1066.
[12] D. Zhao, J. Pan, Y. Zhou, L. Sui, Z. Ye, New types of steel-FRP composite bar with round steel bar inner core: Mechanical properties and bonding performances in concrete, Constr. Build. Mater. 242 (2020).
[13] G. Wu, Z. Sun, Z. Wu, Y. Luo, Mechanical properties of steel-FRP composite bars (SFCBs) and performance of SFCB reinforced concrete structures, Adv. Struct. Eng. 15 (2012) 625–635.
[14] S. Han, A. Zhou, J. Ou, Relationships between interfacial behavior and flexural performance of hybrid steel-FRP composite bars reinforced seawater sea-sand concrete beams, Compos Struct. 277 (2021).
[15] Z. Dong, G. Wu, Y. Xu, Experimental study on the bond durability between steel-FRP composite bars (SFCBs) and sea sand concrete in ocean environment, Constr. Build. Mater. 115 (2016) 277–284.
[16] W. Ge, Y. Wang, A. Ashour, W. Lu, D. Cao, Flexural performance of concrete beams reinforced with steel–FRP composite bars, Arch. Civ. Mech. Eng. 20 (2020) 1–17.
[17] S. Han, C. Fan, A. Zhou, J. Ou, Simplified implementation of equivalent and ductile performance for steel-FRP composite bars reinforced seawater sea-sand concrete beams: equal-stiffness design method, Eng. Struct. 266 (2022).
[18] S. Sun, L. Xing, P. Gui, B. Li, H. Li, L. Zhao, et al., Experimental Study on the Bond Performance of Steel–Basalt Fiber Composite Bars in Concrete, J. Compos Constr. 27 (2023).
[19] Z. Sun, Y. Tang, Y. Luo, G. Wu, X. He, Mechanical properties of steel-FRP composite bars under tensile and compressive loading, Int. J. Polym. Sci. 2017 (2017).
[20] G. Ma, Y. Huang, F. Aslani, T. Kim, Tensile and bonding behaviours of hybridized BFRP–steel bars as concrete reinforcement, Constr. Build. Mater. 201 (2019) 62–71.
[21] Z. Dong, G. Wu, X.-L. Zhao, H. Zhu, J. Lian, Bond durability of steel-FRP composite bars embedded in seawater sea-sand concrete under constant bending and shearing stress, Constr. Build. Mater. 192 (2018) 808–817.
[22] W. Ge, M. Han, Z. Guan, P. Zhang, A. Ashour, W. Li, et al., Tension and bonding behaviour of steel-FRP composite bars subjected to the coupling effects of chloride corrosion and load, Constr. Build. Mater. 296 (2021).
[23] Z. Sun, Y. Yang, W. Qin, S. Ren, G. Wu, Experimental study on flexural behavior of concrete beams reinforced by steel-fiber reinforced polymer composite bars, J. Reinf. Plast. Compos 31 (2012) 1737–1745.
[24] Y. Yang, Z.-y Sun, G. Wu, D.-f Cao, D. Pan, Experimental study of concrete beams reinforced with hybrid bars (SFCBs and BFRP bars), Mater. Struct. 53 (2020).
[25] C. Su, X. Wang, L. Ding, Z. Chen, S. Liu, Z. Wu, Experimental study on the seismic behavior of seawater sea sand concrete beams reinforced with steel-FRP composite bars, Eng. Struct. 248 (2021).
[26] T.-L. Xiao, H.-X. Qiu, J.-L. Li, Seismic behaviors of concrete beams reinforced with steel-FRP composite bars under quasi-static loading, Appl. Sci. 8 (2018) 1913.
[27] E.M.A. Abbas, Y. Ge, Z. Zhang, Y. Chen, A. Ashour, W. Ge, et al., Flexural behavior of UHPC beam reinforced with steel-FRP composite bars, Case Stud. Constr. Mater. 16 (2022).
[28] Z.-Y. Sun, G. Wu, Z.-S. Wu, M. Zhang, Seismic Behavior of Concrete Columns Reinforced by Steel-FRP Composite Bars, J. Compos Constr. 15 (2011) 696–706.
[29] Z. Sun, G. Wu, J. Zhang, Y. Zeng, W. Xiao, Experimental study on concrete columns reinforced by hybrid steel-fiber reinforced polymer (FRP) bars under horizontal cyclic loading, Constr. Build. Mater. 130 (2017) 202–211.
[30] W. Ge, K. Chen, Z. Guan, A. Ashour, W. Lu, D. Cao, Eccentric compression behaviour of concrete columns reinforced with steel-FRP composite bars, Eng. Struct. 238 (2021).
[31] Y.-C. Guo, S.-H. Xiao, J.-J. Zeng, J.-Y. Su, T.-Z. Li, Z.-H. Xie, Behavior of concrete-filled FRP tube columns internally reinforced with FRP-steel composite bars under axial compression, Constr. Build. Mater. 315 (2022).
[32] Z. Sun, Y. Chen, S.-Y. Xu, Y. Sun, G. Wu, Shaking table test of concrete columns hybrid reinforced by steel/FRP bars, J. Build. Eng. 48 (2022).
[33] W. Qin, X. Liu, Z. Xi, Z. Huang, A. Al-Mansour, M. Fernand, Experimental research on the progressive collapse resistance of concrete beam-column sub-assemblages reinforced with steel-FRP composite bar, Eng. Struct. 233 (2021).
[34] Z. Huang, W. Chen, H. Hao, Z. Chen, T.M. Pham, T.T. Tran, et al., Flexural behaviour of ambient cured geopolymer concrete beams reinforced with BFRP bars under static and impact loads, Compos Struct. 261 (2021), 113282.
[35] Z. Huang, W. Chen, H. Hao, R. Aurelio, Z. Li, T.M. Pham, Test of Dynamic Mechanical Properties of Ambient-Cured Geopolymer Concrete Using Split Hopkinson Pressure Bar, J. Mater. Civ. Eng. 34 (2022), 04021440.
[36] Z. Huang, M.Z.N. Khan, W. Chen, H. Hao, Y. Wu, T.M. Pham, et al., Experimental and numerical study of the performance of geopolymer concrete columns reinforced with BFRP bars subjected to lateral impact loading, Constr. Build. Mater. 357 (2022), 129362.
[37] Z. Huang, M.Z.N. Khan, W. Chen, H. Hao, M. Elchalakani, T.M. Pham, Effectiveness of reinforcing methods in enhancing the lateral impact performance of geopolymer concrete column reinforced with BFRP bars, Int J. Impact Eng. 175 (2023), 104544.
[38] Jiangsu Green Materials Vally New Material T&D Co. Ltd (GMV). Steel-FRP Composite Bar. China.
[39] P. Nath, P.K. Sarker, Effect of GGBFS on setting, workability and early strength properties of fly ash geopolymer concrete cured in ambient condition, Constr. Build. Mater. 66 (2014) 163–171.
[40] F. Shi, T.M. Pham, H. Hao, Y. Hao, Post-cracking behaviour of basalt and macro polypropylene hybrid fibre reinforced concrete with different compressive strengths, Constr. Build. Mater. 262 (2020).
[41] J.S. Lawler, D. Zampini, S.P. Shah, Microfiber and macrofiber hybrid fiber-reinforced concrete, J. Mater. Civ. Eng. 17 (2005) 595–604.
[42] J. Branston, S. Das, S.Y. Kenno, C. Taylor, Mechanical behaviour of basalt fibre reinforced concrete, Constr. Build. Mater. 124 (2016) 878–886.
[43] M. Safiuddin, M. Yakhlaf, K.A. Soudki, Key mechanical properties and microstructure of carbon fibre reinforced self-consolidating concrete, Constr. Build. Mater. 164 (2018) 477–488.
[44] ACI 318–14. Building Code Requirements for Structural Concrete (ACI 318–14) and Commentary on Building Code Requirements for Structural Concrete (ACI 318–14). Farmington Hills, MI, USA: American Concrete Institute; 2014.

[45] H. Li, W. Chen, Z. Huang, H. Hao, T.T. Ngo, T.M. Pham, et al., Dynamic response of monolithic and precast concrete joint with wet connections under impact loads, Eng. Struct. 250 (2022).
[46] Z. Li, A. Khennane, P.J. Hazell, A.M. Remennikov, Performance of a hybrid GFRP-concrete beam subject to low-velocity impacts, Compos Struct. 206 (2018) 425–438.
[47] Y. Fujimoto, C. Liu, Y. Tanaka, E. Shintaku, T. Nakanishi, Thorn-shape waveform and double-strike phenomenon seen in the impact force of soft materials, World J. Mech. 5 (2015) 59.